## Title

Technical Note: Iterative megavoltage CT (MVCT) reconstruction using block-matching 3D-transform (BM3D) regularization.



## Journal

Medical Physics, 45(6)

## Authors

Lyu, Qihui
Yang, Chunlin
Gao, Hao
et al.

## Publication Date

2018-06-01

## DOI

10.1002/mp.12916

Peer reviewed

# Technical Note: Iterative megavoltage CT (MVCT) reconstruction using block-matching 3D-transform (BM3D) regularization

Qihui Lyu
*Department of Radiation Oncology, University of California Los Angeles, Los Angeles, CA, USA*

Chunlin Yang
*Sir Run Run Shaw Hospital, Zhejiang University School of Medicine, Institute of Translational Medicine, Zhejiang University, Hangzhou, China*

Hao Gao
*Department of Radiation Oncology, Duke University Medical Center, Durham, NC, USA*

Yi Xue
*Sir Run Run Shaw Hospital, Zhejiang University School of Medicine, Institute of Translational Medicine, Zhejiang University, Hangzhou, China*

Daniel O'Connor
*Department of Radiation Oncology, University of California Los Angeles, Los Angeles, CA, USA*

Tianye Niu
*Sir Run Run Shaw Hospital, Zhejiang University School of Medicine, Institute of Translational Medicine, Zhejiang University, Hangzhou, China*

Ke Sheng[a)]
*Department of Radiation Oncology, University of California Los Angeles, Los Angeles, CA, USA*

(Received 23 November 2017; revised 5 March 2018; accepted for publication 4 April 2018; published 30 April 2018)

**Purpose:** Megavoltage CT (MVCT) images are noisier than kilovoltage CT (KVCT) due to low detector efficiency to high-energy x rays. Conventional denoising methods compromise edge resolution and low-contrast object visibility. In this work, we incorporated block-matching 3D-transform shrinkage (BM3D) transformation into MVCT iterative reconstruction as nonlocal patch-wise regularization.

**Methods:** The iterative reconstruction was achieved by adding to the existing least square data fidelity objective a regularization term, formulated as the L1 norm of the BM3D transformed image. A Fast Iterative Shrinkage-Thresholding Algorithm (FISTA) was adopted to accelerate CT reconstruction. The proposed method was compared against total variation (TV) regularization, BM3D postprocess method, and filtered back projection (FBP).

**Results:** In the Catphan phantom study, BM3D regularization better enhances low-contrast objects compared with TV regularization and BM3D postprocess method at the same noise level. The spatial resolution using BM3D regularization is 2.79 and 2.55 times higher than that using the TV regularization at 50% of the modulation transfer function (MTF) magnitude, for the fully sampled reconstruction and down-sampled reconstruction, respectively. The BM3D regularization images show better bony details and low-contrast soft tissues, on the head and neck (H&N) and prostate patient images.

**Conclusions:** The proposed iterative BM3D regularization CT reconstruction method takes advantage of both the BM3D denoising capability and iterative reconstruction data fidelity consistency. This novel approach is superior to TV regularized iterative reconstruction or BM3D postprocess for improving noisy MVCT image quality.  [https://doi.org/10.1002/mp.12916]

Key words: BM3D, CT, reconstruction

## 1. INTRODUCTION

Megavoltage CT (MVCT) is used in image-guided TomoTherapy treatment but its quality is plagued by high noise level as a result of low detector quantum efficiency (DQE) of high-energy x rays.[1,2] Both postprocessing and iterative reconstruction were used to suppress the noise. In iterative CT reconstruction, regularization terms play an important role.[3] Inspired by the compressed sensing theory, L1-type regularization terms such as total variation (TV) have been widely used in CT iterative reconstructions to preserve image edges.[4–6] Recently, a tensor framelet regularization scheme, the generalization of TV, wavelet, and L1-norm, was proposed by Gao et al. to maintain the object boundary in MVCT reconstruction while suppressing noise.[7] These techniques are effective to remove the image noise and streaking

artifacts due to view aliasing in reconstructed images, but still result in noticeable image resolution loss when noise variation is high as shown in MVCT.

The block-matching 3D-transform shrinkage (BM3D) algorithm was recently proposed and achieved superior image noise suppression relative to local denoising methods by clustering similar but nonlocal 2D image patches into one group and performing denoising within each group.[8,9] Because of the desired denoise performance, BM3D has been used in CT reconstruction. In a naïve fashion, BM3D was applied directly on the CT projection[10] or reconstructed CT images[11–13] as a preprocessing or postprocessing component separate from the reconstruction. These studies showed superior image resolution preservation to local denoising methods but the inherit balance between data fidelity and BM3D regularization was not fully exploited as a single optimization problem. The integrated optimization approach was initially implemented for deblurring and denoising natural images,[14–16] where BM3D was formulated as L1 regularization to encourage data sparsity in the BM3D transformation domain. This method exploited data consistency while suppressing image noise, better preserved image features and outperformed the naïve application. In 2013, Yang et al.[17] used BM3D patches extracted from *a priori* fully sampled images to regularize sparse view reconstruction of a 2D digital phantom. However, iterative CT reconstruction using BM3D on real phantom and patient projections has not been demonstrated. In this study, BM3D regularization was applied to Catphan and patient MVCT reconstruction.

## 2. MATERIALS & METHODS

### 2.A. Problem Formulation

The CT iterative reconstruction with BM3D regularization is formulated as

$$\hat{x} = \underset{x \geq 0}{\operatorname{argmin}} \frac{1}{2}\|Ax - g_2^2\| + \beta H_\mu(\Phi x), \quad (1)$$

where g is the measured projection data, A is the forward projection matrix, $\Phi$ is the BM3D transformation matrix, $\beta$ is the hyperparameter controlling the tradeoff between data fidelity and regularization, and $H_\mu$ is the Huber penalty function with a smoothing parameter $\mu$[18] that approximates the L1 norm, defined as

$$H_\mu(y) = \begin{cases} \frac{1}{2\mu}y^2, & |y| \leq \mu \\ |y| - \frac{\mu}{2}, & |y| > \mu. \end{cases}$$

In Eq. (1), the quadratic data fidelity term minimizes the discrepancy between the measured and the estimated projections, and the regularization term promotes sparsity in the BM3D transformation domain, which subsequently encourages image smoothness and maintains image texture.

As shown in Fig. 1, the workflow involved two main steps. In the first step, a block-matching process was performed on a coarsely reconstructed initial image to generate the matched groups, from which the BM3D analysis matrix $\Phi$ was constructed. In the second step, matrix $\Phi$ was utilized in Eq. (1) for iterative reconstruction.

### 2.B. Construction of BM3D transformation matrix

The block-matching was performed on the initial CT images from TV reconstruction, on which each reference patch $P_r (r = 1, 2, \ldots, R)$, with size $n^p$ by $n^p$ and a separation distance $n^d$ in both the row and column directions, is denoted by the index of the voxel at the left upper corner. For each $P_r$, a nonlocal searching procedure is performed within the $P_r$-centered $n^w$-by-$n^w$ window on the initial CT image to obtain a group of similar patches $G_r = \{S_{r,j=1}, S_{r,j=2}, \cdots, S_{r,j=J}\}$ to $P_r$ with respect to Euclidean distance. Let x be the vectorized MVCT image with dimension N. An indicator matrix $I_{r,j}$ with dimension $(n^p)^2$-by is defined for the $j^{th}$ patch in the $r^{th}$ group, such that $I_{r,j} \cdot x$ is a vector containing every pixel in the similar patch $S_{r,j}$. The indicator matrix $I_r$ for group $G_r$ is a concatenation of all $I_{r,j} (j = 1, 2, \ldots, J)$, and the matrix-vector product $I_r \cdot x$ provides the vectorized group $G_r$.

Aside from the indicator matrix, two independent linear transformation matrices $T_1$ and $T_2$ are utilized in the construction of BM3D analysis matrix. $T_1$ is the 1D Hadamard transformation matrix that performs interpatch transformation across different patches within one group. $T_2$ is the 2D Haar wavelet matrix for intrapatch transformation within each patch. $T_1$ and $T_2$ together implement a 3D transformation on the group $G_r$ that transforms image patches in $G_r$ to the BM3D spectra, with spectra coefficients given by

$$\omega_r = (T_1 \otimes T_2) \cdot (I_r \cdot x)$$

The joint BM3D spectra are a concatenation of the BM3D spectra for all groups. By defining the BM3D analysis matrix $\Phi$ as

$$\Phi = \begin{bmatrix} (T_1 \otimes T_2) \cdot I_{r=1} \\ (T_1 \otimes T_2) \cdot I_{r=2} \\ \vdots \\ (T_1 \otimes T_2) \cdot I_{r=R} \end{bmatrix},$$

the joint BM3D spectra are related to the vectorized image x by $\omega = \Phi x$.

### 2.C. Minimization of objective function

The objective function in Eq. (1) was minimized using a Fast Iterative Shrinkage-Thresholding Algorithm (FISTA), a fast proximal method that solves optimization problem in the form of

$$\text{minimize} \quad F(x) + G(x),$$

where F is convex and differentiable function with a Lipschitz continuous gradient, and G is a convex simple function in that its proximal operator can be evaluated efficiently. The proximal operator is evaluated through[18]

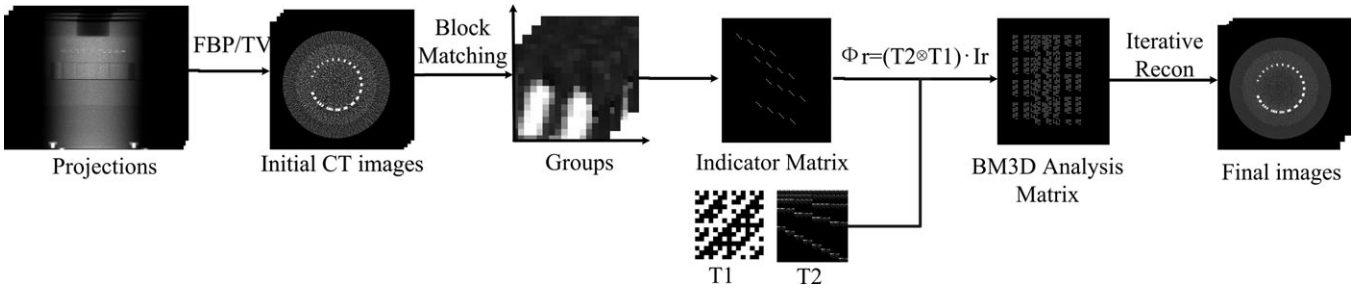


FIG. 1. Workflow of the MVCT iterative reconstruction using BM3D regularization.

$$\mathrm{prox}_{tG}(x) = \underset{z}{\mathrm{argmin}} \left( G(z) + \frac{1}{2t}\|z - x\|_2^2 \right).$$

Algorithm 1 summarizes the FISTA with line search algorithm, where the main operation in each iteration of FISTA are the evaluation of the proximal operator of G and the gradient of F.

**Algorithm 1: FISTA with line search.**

*Pseudocode for FISTA with line search*

*Initialize* $x_0 := 0$, $v_0 := x_0$, $t_0 > 0$, $r_1 > 1$, $r_2 > 1$
*for* $k = 1, 2, \ldots$ *do*
  $t := r_1 t_{k-1}$
  *Repeat*
    $\theta := \begin{cases} 1 & if \ \ k = 1 \\ positive\ root\ of\ t_{k-1}\theta^2 = t\theta_{k-1}^2(1-\theta) & if \ \ k > 1 \end{cases}$
    $y := (1-\theta)x_{k-1} + \theta v_{k-1}$
    $x := prox_{tG}(y - t\nabla F(y))$
  *break if* $F(x) \le F(y) + < \nabla F(y), x - y > + \frac{1}{2t}\|x - y\|_2^2$
  $t := t/r_2$
 $t_k := t$
 $\theta_k := \theta$
 $v_k := x_k + \frac{1}{\theta_k}(x - x_k)$
 *break if* $\frac{\|x - x_k\|}{\|x_k\|} \le \epsilon$
 $x_k := x$
*end for*
return **x**

The proposed optimization problem Eq. (1) is presented in a canonical FISTA form by defining:

$$F(x) = \frac{1}{2}\|Ax - g\|_2^2 + \beta H(\Phi x),$$

$$G(x) = I_+(x) = \begin{cases} 0 & \text{if } x \ge 0 \\ \infty & \text{otherwise} \end{cases}.$$

The proximal operator of G simply projects onto the non-negative orthant:

$$\mathrm{prox}_{tG}(x) = P_+(x) = \max(x, 0),$$

and the gradient of F is given by

$$\nabla F(x) = A^T(Ax - g) + \frac{\beta}{\mu}\Phi^T P_{[-\mu,\mu]}(\Phi x).$$

This allows a direct application of FISTA to our formulation.

### 2.D. Evaluation

A Siemens imaging quality phantom,[19] a head and neck (H&N) patient, and a prostate patient was scanned on an onboard TomoTherapy imaging system[20] with a 3.5 MV helical fan beam. A total number of 800 projections were acquired. The proposed method is compared with Filtered Back Projection (FBP), TV, and BM3D postprocessing methods, where the BM3D postprocess performs the BM3D denoising filter on a FBP-reconstructed CT image. Evaluation includes both full sampled reconstruction and down-sampled reconstruction, where 25% of the uniformly sampled projections are utilized. The task-based modulation transfer function (MTF)[21] is evaluated for comparison of image resolution across both linear and nonlinear reconstruction methods.

## 3. RESULTS

### 3.A. Phantom study

The reconstruction results using BM3D regularization, TV, BM3D postprocess and FBP on a line pair slice and a contrast rod slice of the Siemens imaging quality phantom are shown in Figs. 2 and 3 respectively, for both fully sampled reconstruction and down-sampled reconstruction. The image noise, computed as the standard deviation (STD) within the squares on Figs. 2(d1) and 3(d1), is kept at the same level across all reconstruction methods except for FBP. TV reconstruction loses the fine feature as shown by the 8th line pair on the 800 projection image and the 7th line pair on the 200 projection image, whereas these line pairs are distinguishable on images reconstructed from other methods. BM3D postprocess method achieves comparably high spatial resolution as the BM3D regularization methods, as evaluated by these high-contrast line pairs, but the postprocessing method amplifies streaking artifacts, [Fig. 2(c2)], which originates from the noisy FBP image in Fig. 2(d2), due to the lack of iterative fidelity penalty in this approach. Compared to other methods, the BM3D regularization method is able to maintain image spatial resolution while removing both the noise and artifacts.

The contrast rod slice compares performance on high- and low-contrast objects across different reconstruction methods. Both TV and BM3D postprocess are less effective at

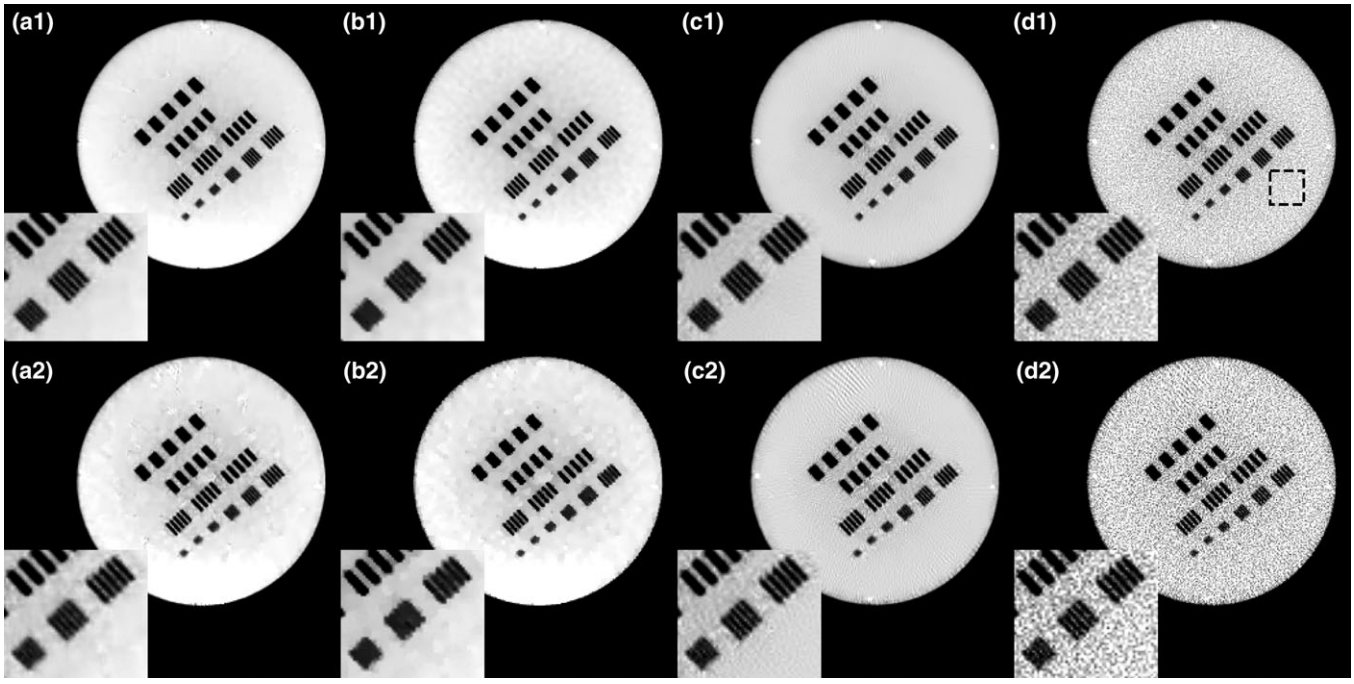


FIG. 2. Resolution slice reconstructed from (a) BM3D regularization, (b) TV, (c) BM3D postprocess, and (d) FBP using (1) 800 projections and (2) 200 projections, respectively. Zoom-in details for the 6th–8th line pairs are shown in the left lower corner. The images from BM3D regularization, TV, and BM3D postprocess are under the same noise level.

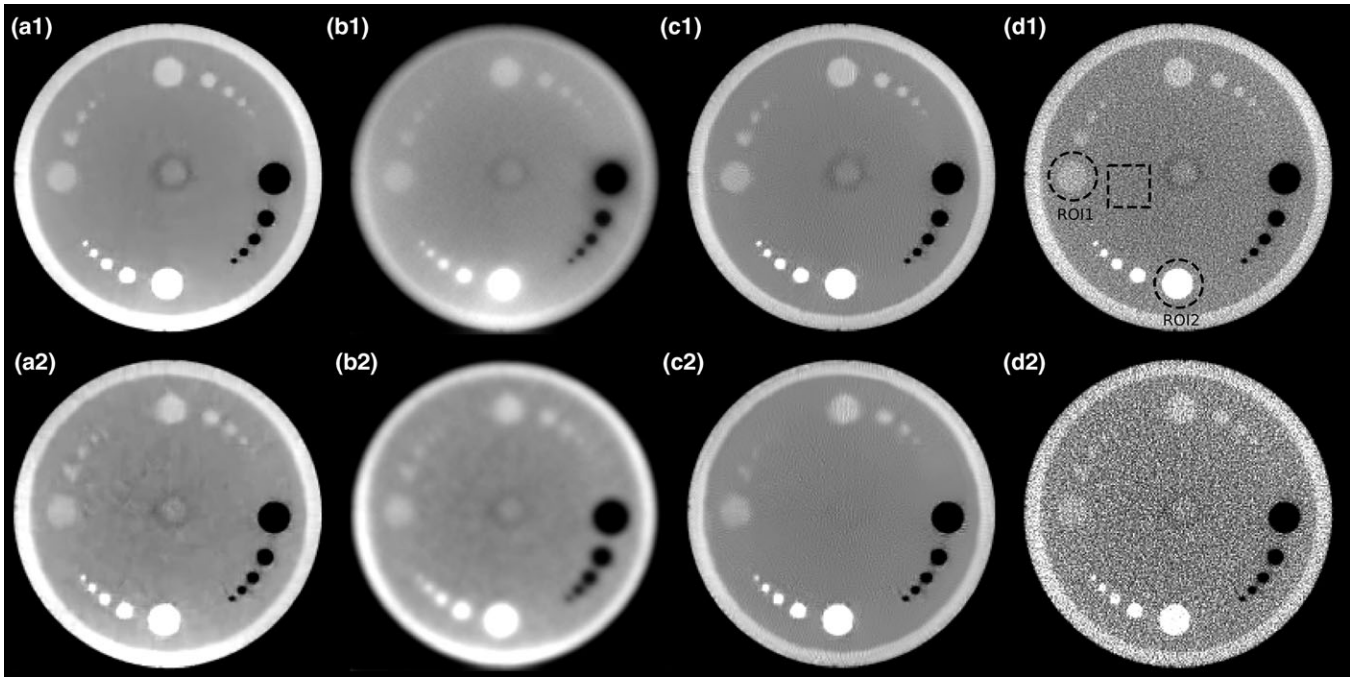


FIG. 3. Contrast rod slice reconstructed from (a) BM3D regularization, (b) TV, (c) BM3D postprocess, and (d) FBP using (1) 800 projections and (2) 200 projections, respectively. The images from BM3D regularization, TV, and BM3D postprocess are under the same noise level.

preserving low-contrast objects while removing the image noise, whereas the BM3D regularization image is able to distinguish low-contrast fine structures that were obscured by the noise in the FBP images. Table I presents the quantitative CNR values evaluated on the contrast rod object indicated by the region-of-interest (ROI) with label 1 on Fig. 3(d1).

Image resolution comparison across BM3D regularization, TV, and BM3D postprocess methods under the same noise level is presented by the line profile plots of the 6$^{th}$ line pair in Fig. 4 and the MTF plots in Fig. 5, evaluated basing on the highest contrast object (ROI2) on Fig. 3(d1). Figures 4 and 5 show that, for high-contrast objects, with equal image

TABLE I. The CNR for the contrast slice with the ROI1 indicated in Fig. 3(d1).

| CNR | BM3D regularization | TV | BM3D postprocessing | FBP |
|---|---|---|---|---|
| 800 Projections | 372.10 | 222.10 | 300.61 | 48.91 |
| 200 Projections | 235.09 | 230.75 | 203.34 | 14.47 |

noise suppression, both the BM3D postprocess and the BM3D regularization methods maintained resolution comparable to the FBP, whereas the TV regularization degraded the resolution. At 50% of the MTF magnitude, the spatial resolution using BM3D regularization is 5.00 and 4.33 lp/cm, whereas that of using TV is 1.79 and 1.70 lp/cm, for the fully sampled reconstruction and down-sampled reconstruction, respectively.

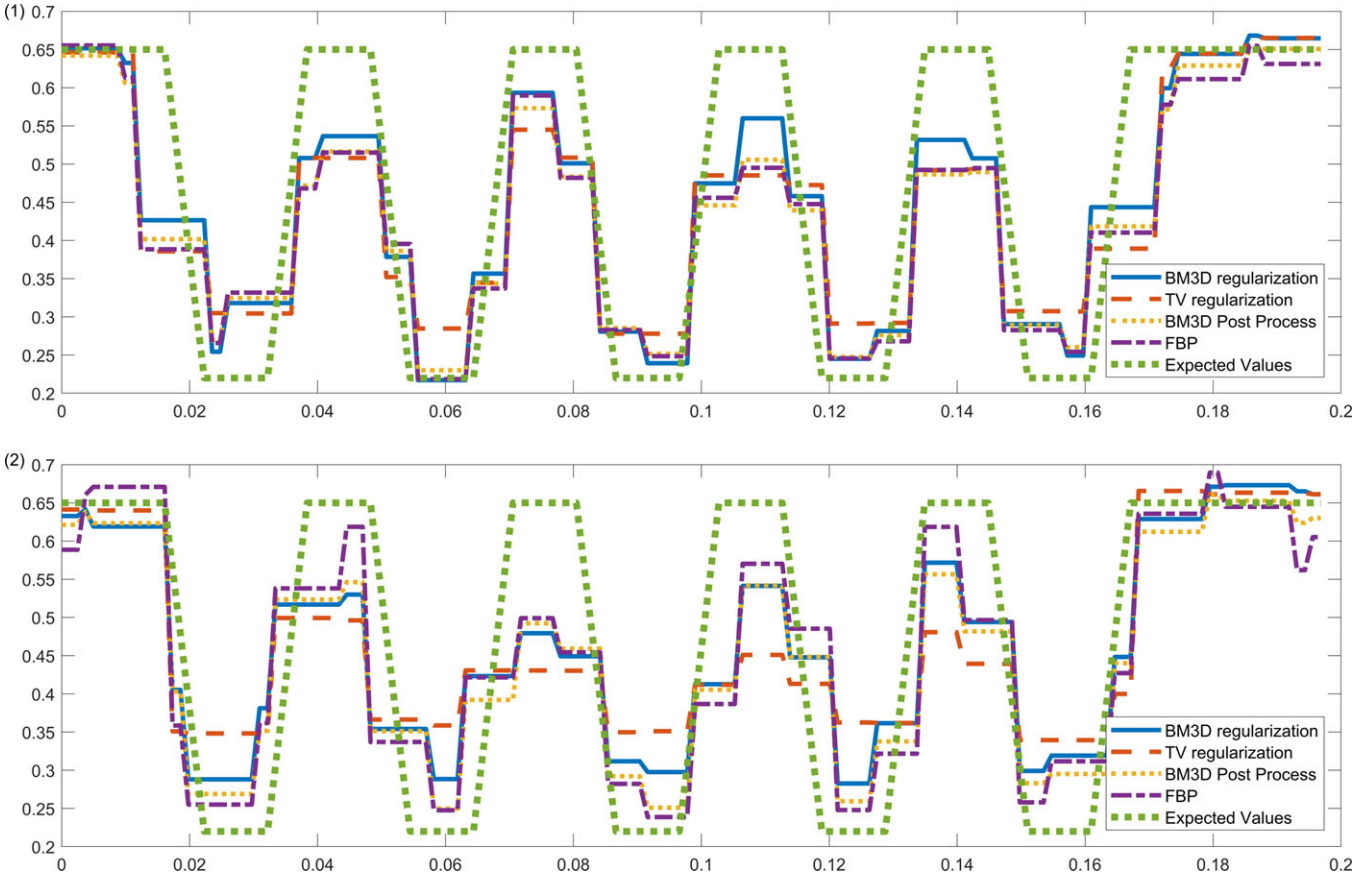


FIG. 4. Cross-line plots of the 6th line pair on the resolution slice for all methods and the expected values, using (1) 800 projections and (2) 200 projections. The images from BM3D regularization, TV, and BM3D postprocess are under the same noise level. [Color figure can be viewed at wileyonlinelibrary.com]

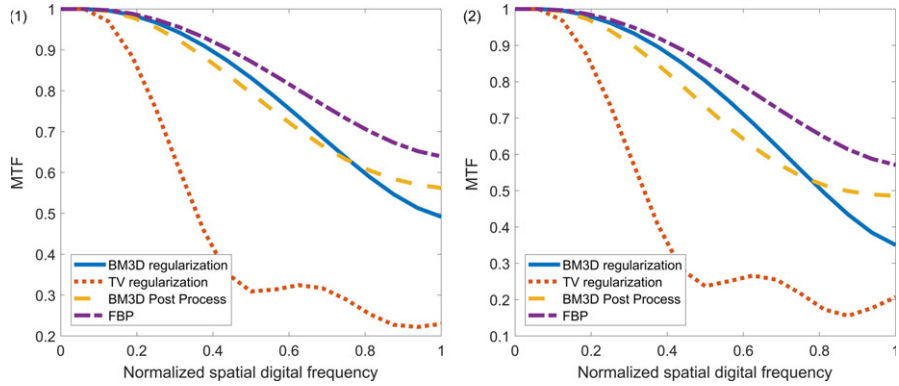


FIG. 5. MTF of the MVCT images reconstructed from BM3D regularization, TV, BM3D postprocess, and FBP using (1) 800 projections and (2) 200 projections. The images from BM3D regularization, TV, and BM3D postprocess are under the same noise level. [Color figure can be viewed at wileyonlinelibrary.com]

Figure 6 shows the tradeoff between image noise and resolution for different reconstruction methods. The image noise is computed as the STD of the square on Fig. 3 (d1), and the image resolution is calculated as the area under the MTF curve, where the task-based MTF is evaluated on the object in ROI2 on Fig. 3 (d1). Across a suitable range of image noise, both the BM3D regularization and the BM3D postprocess were able to maintain a comparably high image resolution compared with TV, for both the fully sampled reconstruction and down-sampled reconstruction. The images shown in Fig. 3 corresponds to the noise STD at 0.14 and 0.18 for 800 projections and 200 projections, respectively.

### 3.B. Patient study

The reconstruction results for a H&N patient slice and a prostate patient slice using BM3D regularization, TV, BM3D postprocess, and FBP are shown in Figs. 7 and 8 respectively, for both fully sampled reconstruction and down-sampled reconstruction. The image noise, computed as the STDs of

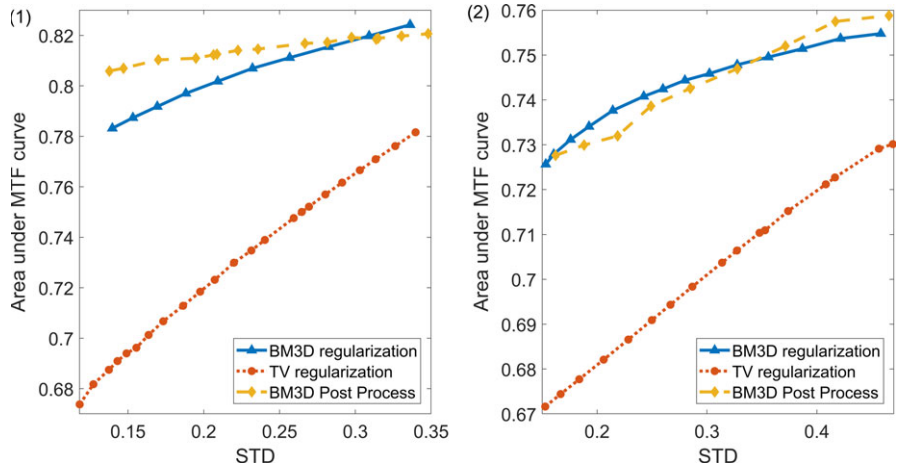


FIG. 6. The resolution vs noise curve of BM3D regularization, TV, and BM3D postprocess using (1) 800 projections and (2) 200 projections. The resolution is computed as the area under the MTF curve, evaluated on the ROI2 on Figure 3 (d1), and the image noise is computed as the STD of the square on Figure 3 (d1). [Color figure can be viewed at wileyonlinelibrary.com]

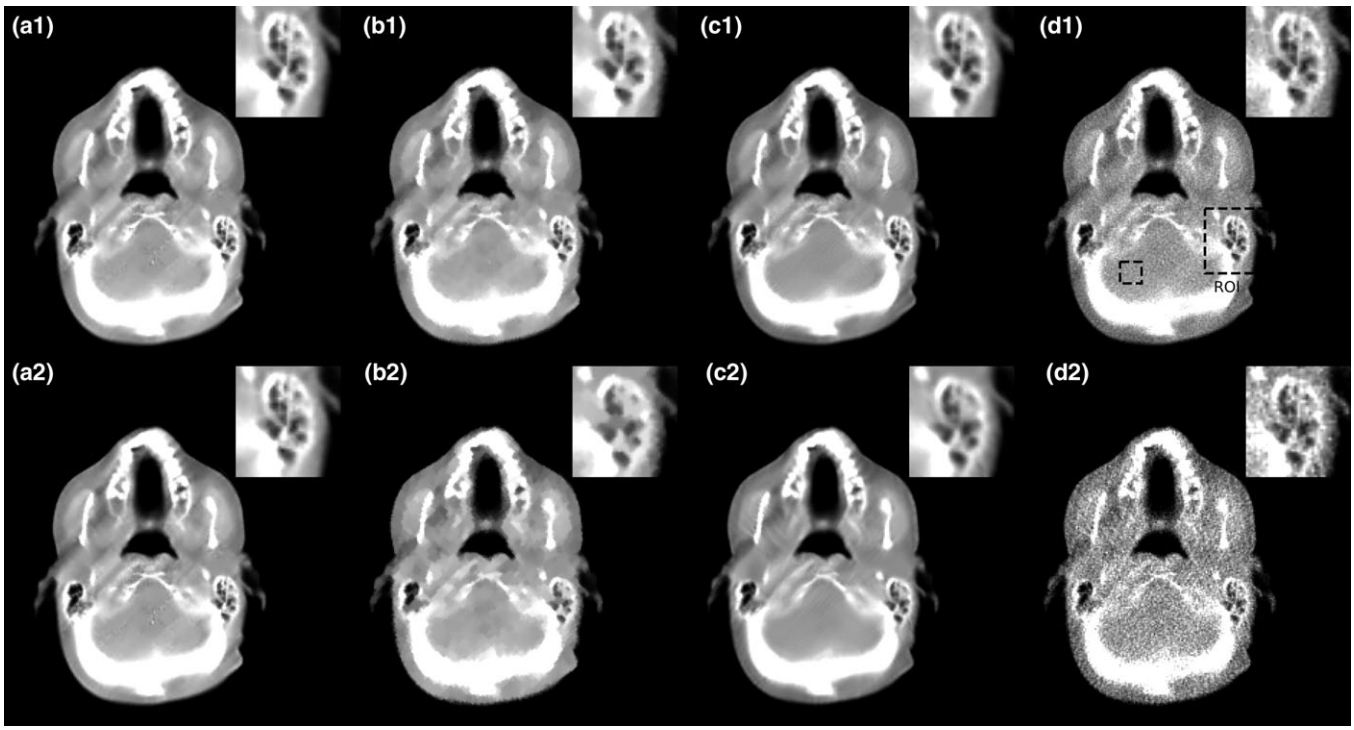


FIG. 7. H&N images with zoom-in displays of ROI reconstructed from (a) BM3D regularization, (b) TV, (c) BM3D postprocess, and (d) FBP using (1) 800 projections and (2) 200 projections, respectively.

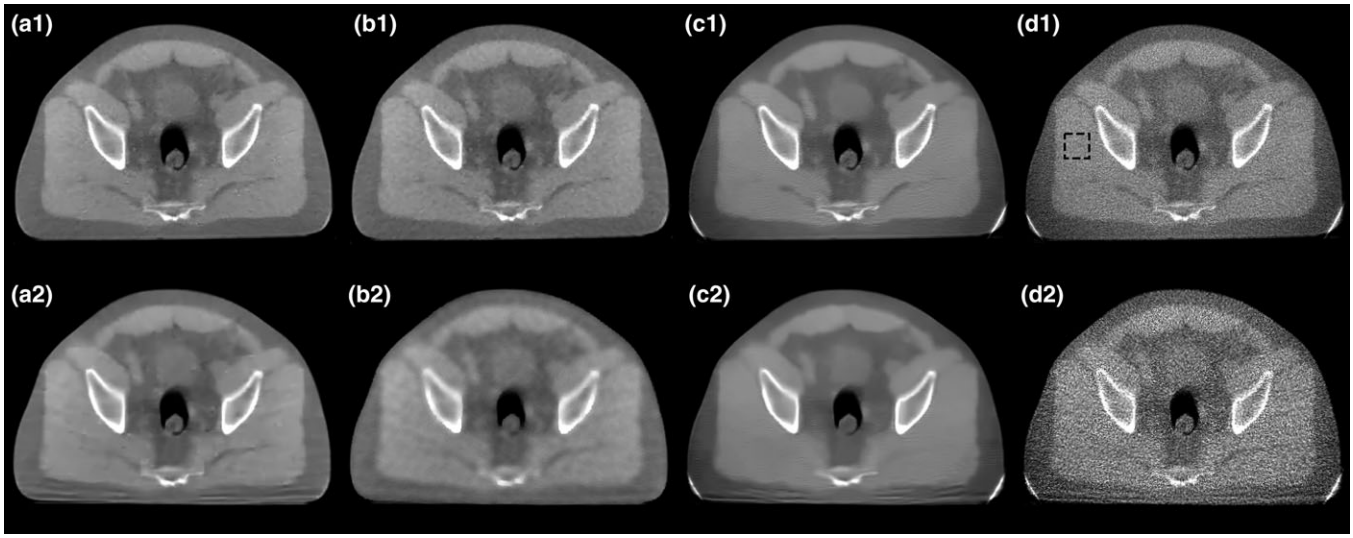


FIG. 8. Prostate images reconstructed from (a) BM3D regularization, (b) TV, (c) BM3D postprocess, and (d) FBP using (1) 800 projections and (2) 200 projections, respectively.

the squares on Fig. 7(d1) and 8(d1), is kept at the same level across all reconstruction methods except for FBP. TV images lose fine bone structures as shown in the zoom-in ROI displays of H&N patient in Fig. 7, and produce cartoon-like artifacts characteristic to TV regularization. BM3D postprocess images are able to preserve image spatial resolutions in the high-contrast region comparable to BM3D regularization and FBP, but are less effective in preserving the low-contrast structures, shown in the zoom-in ROIs. For the prostate patient, the TV images showed more blurred bony boundaries. Compared with BM3D regularization, the BM3D postprocess results in worse soft tissue contrast, as shown in Fig. 8(c2), and magnifies the FBP image artifacts.

## 4. DISCUSSION

CT imaging dose is a concern for diagnostic imaging and image-guided radiation therapy, motivating the development of low-dose CT. In practice, imaging dose reduction is achieved using sparse projection sampling and/or reduced x-ray tube current.[22,23] Due to the ill-conditioned system matrix brought by the heavily undersampled data and/or high noise in low-dose CT imaging, iterative reconstruction has shown superiority in image artifact reduction and noise control in comparison to the analytical filtered-backprojection (FBP) algorithm since the former incorporates physical constraints and image features into the iterative framework as regularization terms.[3] Because of the low DQE, MVCT can be a viewed as a special case of low-dose CT that can benefit from iterative CT reconstruction.

In this work, we for the first time implemented nonlocal BM3D regularization as L1 regularization for raw CT data reconstruction. Compared with TV regularization, both BM3D postprocess and regularization are more effective in maintaining the resolution while reducing the noise. BM3D regularization, however, is better at enhancing low-contrast conspicuity and controlling artifacts than BM3D postprocess due to the iterative application of the fidelity term.

One limitation of the BM3D regularization is its higher computational cost. Compared with the 2D natural image processing reported by Danielyan et al.,[14] the CT reconstruction problem is several orders of magnitude greater. The previous method of solving BM3D regularized iterative reconstruction using ADMM,[17] except for the difference of relying on *a priori* data for reconstruction, is impractically slow for real patient data. In this study, to improve the computational speed, the optimization problem was solved using FISTA,[24] a fast proximal gradient method. On one hand, FISTA requires only the multiplication with the system matrix and its transpose at each iteration, substantially reduces the computational costs as compared with other first order methods such as the alternating direction method of multipliers (ADMM).[25] On the other hand, it achieves a convergence rate of $O\left(\frac{1}{k^2}\right)$, a significant improvement over the $O\left(\frac{1}{k}\right)$ convergence rate of most other first-order methods such as ADMM and Chambolle–Pock algorithm.[26] In addition, to reduce matrix multiplication time and reduce the memory usage, the BM3D analysis matrix was implemented as sequential multiplication of small transformation matrices in different dimensions.[8] With these acceleration methods, reconstruction for one image slice currently takes approximately 30 s with BM3D regularization, whereas FBP reconstruction and TV reconstruction takes less than 0.2 and 3 s, respectively, on a Intel Core i7-7700K CPU with 64 GB RAM and a GTX TITAN X. As a future development, the embarrassingly parallelizable matrix multiplication time can be further reduced with hardware acceleration techniques, e.g., graphics processing unit (GPU).[27]

## 5. CONCLUSION

We proposed a novel iterative reconstruction method for MVCT using the BM3D regularization. The method takes

advantage of the BM3D denoising capability and formulate it as an L1 type regularization. At the same level of noise suppression, BM3D regularization is remarkably more effective than TV regularization in maintaining the resolution and enhancing low-contrast conspicuity. Compared with BM3D postprocess, BM3D regularization better improves low-contrast conspicuity and controls artifacts.

## ACKNOWLEDGMENTS

This research is supported by DOE Grants No. DE-SC0017057 and DE-SC0017687, and NIH Grant R44CA183390, R01CA188300, and R43CA183390.

## CONFLICT OF INTEREST

The authors have no conflicts to disclose.

[a]Author to whom correspondence should be addressed. Electronic mail: ksheng@mednet.ucla.edu

## REFERENCES

1. Beavis AW. Is tomotherapy the future of IMRT? *Br J Radiol*. 2004;77:285–295.
2. Yartsev S, Kron T, Van Dyk J. Tomotherapy as a tool in image-guided radiation therapy (IGRT): theoretical and technological aspects. *Biomed Imaging Interv J*. 2007;3:e16.
3. Bian J, Siewerdsen JH, Han X, et al. Evaluation of sparse-view reconstruction from flat-panel-detector cone-beam CT. *Phys Med Biol*. 2010;55:6575–6599.
4. LaRoque SJ, Sidky EY, Pan X. Accurate image reconstruction from few-view and limited-angle data in diffraction tomography. *J Opt Soc Am A Opt Image Sci Vis*. 2008;25:1772–1782.
5. Chen G-H, Tang J, Leng S. Prior image constrained compressed sensing (PICCS): a method to accurately reconstruct dynamic CT images from highly undersampled projection data sets. *Med Phys*. 2008;35:660–663.
6. Tian Z, Jia X, Yuan K, Pan T, Jiang SB. Low-dose CT reconstruction via edge-preserving total variation regularization. *Phys Med Biol*. 2011;56:5949–5967.
7. Gao H, Qi XS, Gao Y, Low DA. Megavoltage CT imaging quality improvement on TomoTherapy via tensor framelet. *Med Phys*. 2013;40:81919.
8. Lebrun M. An analysis and implementation of the BM3D image denoising method. *Image Process Line*. 2012;2:175–213.
9. Dabov K, Foi A, Katkovnik V. Image denoising by sparse 3D transformation-domain collaborative filtering. *IEEE Trans Image Process*. 2007;16:1–16.
10. Huang J, Ma J, Liu N, Feng Q, Chen W. Projection data restoration guided non-local means for low-dose computed tomography reconstruction. In: *2011 IEEE International Symposium on Biomedical Imaging: From Nano to Macro*, Chicago, IL; 2011: 1167–1170.
11. Sheng K, Gou S, Wu J, Qi SX. Denoised and texture enhanced MVCT to improve soft tissue conspicuity. *Med Phys*. 2014;41:101916.
12. Trinh H, Luong M, Rocchisani J, Dibos F. *An optimal weight method for CT image denoising*; 2012.
13. Kang D, Slomka P, Nakazato R, et al. *Image denoising of low-radiation dose coronary CT angiography by an adaptive block-matching 3D algorithm*; 2013.
14. Danielyan A, Katkovnik V, Egiazarian K. BM3D frames and variational image deblurring. *IEEE Trans Image Process*. 2012;21:1715–1728.
15. Katkovnik V, Danielyan A, Egiazarian K. *Decoupled inverse and denoising for image deblurring: Variational BM3D-frame technique*. Proc. - Int. Conf. Image Process. ICIP 3453–3456, 2011.
16. Danielyan A, Katkovnik V, Egiazarian K. *Image deblurring by augmented langrangian with Bm3D frame prior*. Third Work. Inf. Theor. Methods Sci. Eng., 2010.
17. Yang L, Getreuer P, Linghong Z. Sparse-view cone-beam CT reconstruction via previous normal dose scan induced BM3D-frame regularization method. In: *12th Int. Meet. Fully Three-Dimensional Image Reconstr. Radiol. Nucl. Med.*, Conference Proceedings, Lake Tahoe, CA; 2013: 537–540.
18. Parikh N, Boyd S. Proximal algorithms. *Found Trends Optim*. 2013;1:123–231.
19. Gayou O, Miften M. Commissioning and clinical implementation of a mega-voltage cone beam CT system for treatment localization. *Med Phys*. 2007;34:3183–3192.
20. Moore KL, Palaniswaamy G, White B, Goddu SM, Low DA. Fast, low-dose patient localization on TomoTherapy via topogram registration. *Med Phys*. 2010;37:4068–4077.
21. Richard S, Husarik DB, Yadava G, Murphy SN, Samei E. Towards task-based assessment of CT performance: system and object MTF across different reconstruction algorithms. *Med Phys*. 2012;39:4115–4122.
22. Pouliot J, Bani-Hashemi A, Chen J, et al. Low-dose megavoltage cone-beam CT for radiation therapy. *Int J Radiat Oncol Biol Phys*. 2005;61:552–560.
23. Wang J, Li T, Liang Z, Xing L. Dose reduction for kilovotage cone-beam computed tomography in radiation therapy. *Phys Med Biol*. 2008;53:2897–2909.
24. Beck A, Teboulle M. A fast iterative shrinkage-thresholding algorithm. *Soc Ind Appl Math J Imaging Sci*. 2009;2:183–202.
25. Boyd S. *Alternating direction method of multipliers*. Proc. 51st IEEE Conf. Decis. Control 3(1), 1–44, 2011.
26. Chambolle A, Pock T. A first-order primal-dual algorithm for convex problems with applications to imaging. *J Math Imaging Vis*. 2011;40:120–145.
27. Baskaran MM. *Optimizing sparse matrix-vector multiplication on GPUs using compile-time and run-time strategies*. IBM Res Rep, 24704; 2008.